

# Molecular Dynamic Simulation To Reveal the Mechanism Underlying MGL-3196 Resistance to Thyroxine Receptor Beta

Yi Lu,\* Chun Chen, Deyi Zhuang, and Liling Qian\*

Cite This: *ACS Omega* 2024, 9, 20957–20965

Read Online

ACCESS |



Metrics &amp; More

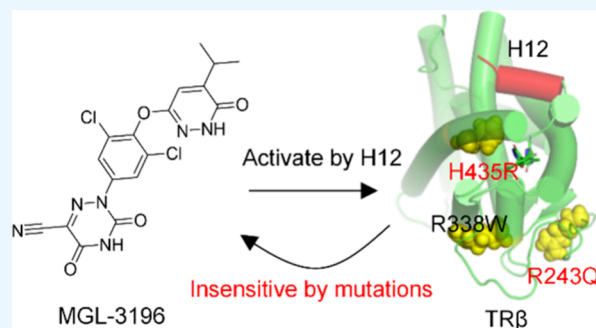


Article Recommendations



Supporting Information

**ABSTRACT:** Thyroxine receptor beta (TR $\beta$ ) is a ligand-dependent nuclear receptor that participates in regulating multiple biological processes, particularly playing an important role in lipid metabolism regulation. TR $\beta$  is currently a popular therapeutic target for non-alcoholic steatohepatitis (NASH), while no drugs have been approved to treat this disease. MGL-3196 (Resmetirom) is the first TR $\beta$  agonist that has succeeded in phase III clinical trials for the treatment of NASH; therefore, studying its molecular mechanism of action is of great significance. In this study, we employed molecular dynamic simulation to investigate the interaction mode between MGL-3196 and TR $\beta$  at the all-atom level. More importantly, by comparing the binding patterns of MGL-3196 in several prevalent TR $\beta$  mutants, it was identified that the mutations R243Q and H435R located, respectively, around and within the ligand-binding pocket of TR $\beta$  cause TR $\beta$  to be insensitive to MGL-3196. This indicates that patients with NASH carrying these two mutations may exhibit resistance to the medication of MGL-3196, thereby highlighting the potential impact of TR $\beta$  mutations on TR $\beta$ -targeted treatment of NASH and beyond.



and TR $\beta$ . The issue of low subtype selectivity has led to the development of compounds with high TR $\beta$  selectivity, such as MB07811<sup>12,13</sup> and MGL-3196<sup>14</sup> (Figure 1), which are currently being studied in phase II/III clinical trials. Among them, MGL-3196 is approaching the primary end point and critical secondary end point in phase III clinical trials for the treatment of NASH.<sup>15–17</sup> However, a noteworthy problem is the frequent TR $\beta$  mutations in patients that generally lead to hormone resistance. Most mutations are located on exons 9 and 10 that encode LBD. Mechanically, mutations can affect the binding of thyroid hormones to TR $\beta$ , which makes TR $\beta$  insensitive to thyroid hormones.<sup>18–20</sup> The impaired sensitivity of TR $\beta$  to thyroid hormones further induces the development of hormone resistance. Therefore, it is worth paying more attention to the TR $\beta$  mutations that may influence the therapeutic effects of TR $\beta$  agonists. To this end, people have attempted to develop new TR $\beta$  agonists that can combat specific mutations. For example, Koh et al. discovered two compounds, QH2<sup>19</sup> (Figure 1) and QH13<sup>20</sup> (Figure 1), which can maintain the activation of H435A and H435Y mutants, respectively. Recently, Xu and co-workers discovered a TR $\beta$

## 1. INTRODUCTION

Thyroid hormone receptors (TRs) belong to the ligand-dependent nuclear receptor superfamily and are involved as transcription factors in regulating multiple biological processes, such as cell growth, development, heart rate, lipid metabolism, and bone density.<sup>1–3</sup> TR family consists of two members, namely TR $\alpha$  and TR $\beta$ . TR $\alpha$  is mainly expressed in the tissues of the heart and bones, while TR $\beta$  is particularly expressed in the liver. TRs are regulated by endogenous thyroid hormones, including triiodothyronine (T3, Figure 1) and thyrotropin (T4, Figure 1). T3 and T4 bind to the ligand-binding domain (LBD) of TRs, thus recruiting coactivators (such as SRC-1) and regulating the expression of genes related to lipid metabolism and weight control.<sup>4–6</sup> Its activation can decrease the level of low-density lipoprotein (LDL) and cholesterol and can promote the liver metabolism rate, leading to weight loss. However, hypothyroidism is an important risk factor for NAFLD, including NASH, and is very common in patients with NAFLD.<sup>7</sup> Impaired thyroid action in the liver accelerates the progression of NAFLD.<sup>8</sup> This link spurs TR-targeted treatment of NASH. Increasing evidence shows that TR $\beta$  agonist is effective for the treatment of NASH. In addition, excessive activation of TR $\beta$  is extensively associated with fibrosis-related diseases, such as liver<sup>9</sup> and pulmonary fibrosis.<sup>10</sup> This signifies TR $\beta$  as a pan-target for various diseases.

Reviewing the history of TR $\beta$  agonists, the majority are thyroid hormone analogs, such as GC-1 and KB-141 (Figure 1),<sup>11</sup> but these compounds can simultaneously activate TR $\alpha$

and TR $\beta$ . The issue of low subtype selectivity has led to the development of compounds with high TR $\beta$  selectivity, such as MB07811<sup>12,13</sup> and MGL-3196<sup>14</sup> (Figure 1), which are currently being studied in phase II/III clinical trials. Among them, MGL-3196 is approaching the primary end point and critical secondary end point in phase III clinical trials for the treatment of NASH.<sup>15–17</sup> However, a noteworthy problem is the frequent TR $\beta$  mutations in patients that generally lead to hormone resistance. Most mutations are located on exons 9 and 10 that encode LBD. Mechanically, mutations can affect the binding of thyroid hormones to TR $\beta$ , which makes TR $\beta$  insensitive to thyroid hormones.<sup>18–20</sup> The impaired sensitivity of TR $\beta$  to thyroid hormones further induces the development of hormone resistance. Therefore, it is worth paying more attention to the TR $\beta$  mutations that may influence the therapeutic effects of TR $\beta$  agonists. To this end, people have attempted to develop new TR $\beta$  agonists that can combat specific mutations. For example, Koh et al. discovered two compounds, QH2<sup>19</sup> (Figure 1) and QH13<sup>20</sup> (Figure 1), which can maintain the activation of H435A and H435Y mutants, respectively. Recently, Xu and co-workers discovered a TR $\beta$

Received: January 3, 2024

Revised: April 17, 2024

Accepted: April 19, 2024

Published: May 1, 2024



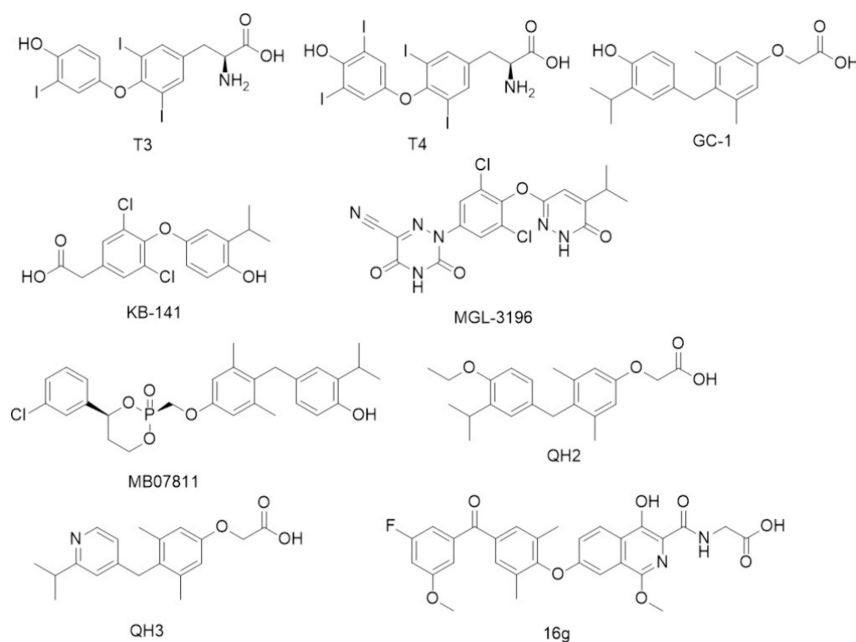


Figure 1. Structures of available TR $\beta$  agonists.

agonist, 16g, which is sensitive to the H435R mutation (Figure 1).<sup>21</sup> However, the impact of TR $\beta$  mutations on the activity of MGL-3196 has not been systematically studied despite its effectiveness in clinical trials.

In this study, we aim to address the queries regarding the binding of MGL-3196 with TR $\beta$  and the impact of hormone-resistant mutations on MGL-3196-mediated TR $\beta$  activation. Molecular dynamics is a potent simulation tool commonly employed to investigate the binding between proteins and ligands. In contrast to the X-ray diffraction structure, which can only capture the static conformation of proteins, molecular dynamic simulations can furnish more dynamic information about the protein–ligand binding. The accessibility of TR $\beta$  crystal structures merely offers a reliable starting conformation for molecular dynamics. Previously, certain studies have explored the binding mechanism of TR $\beta$  antagonists via molecular dynamics.<sup>22</sup> In this study, we utilized molecular dynamics to simulate the binding state of MGL-3196 with wild-type and multiple LBD mutants at the all-atom level. We analyzed its binding mode and the effect of mutations on the maintenance of the TR $\beta$  active conformation with MGL-3196. It is well-known that the helix 12 (H12) at the AF-2 site of the LBD,<sup>23</sup> which is highly conserved in nuclear receptors, is crucial for TR $\beta$  activation by recruiting effector proteins. Consequently, the effect of mutations on H12 under the binding of MGL-3196 was specifically investigated to uncover how TR $\beta$  mutations affect MGL-3196-mediated TR $\beta$  activation through this helix.

## 2. METHODS

**2.1. Protein Preparation.** We extracted the crystal structures coded 3GWS and 1N46 from the RCSB PDB database<sup>24</sup> (<https://www.rcsb.org/>). Among them, 3GWS<sup>25</sup> is the crystal complex structure of thyroid hormone T3, and 1N46<sup>26</sup> is the crystal complex structure of an MGL-3196 derivative (Figure S1). We used H++<sup>27</sup> (<http://newbiophysics.cs.vt.edu/h++/>) to prepare the protein by removing salt ions and crystallized water molecules from the protein, and

correcting nonstandard amino acids with missing atoms or chemical modifications to standard amino acids. Then, hydrogen atoms were added to all heavy atoms at pH 7.0.

Considering that there are no reported crystal structures of TR $\beta$  mutants, we constructed the protein structures of the mutants manually. We selected high-frequent mutations R243Q, R338W, and H435R in clinical patients,<sup>28</sup> all of which can induce thyroid hormone resistance and are located at the N-terminus, central, and C-terminus of the LBD sequence, respectively. Due to the similarity between the ligands within the crystal structures of 1N46 and MGL-3196, we performed manual mutations on the basis of this protein structure. Finally, we constructed five complex structures for simulation, including T3 and MGL-3196-bound wild-type structures and three MGL-3196-bound mutant structures. In addition, the apo structure of the wild-type protein was generated by directly removing the ligand from the crystal structure of 1N46.

**2.2. Ligand Preparation.** Because MGL-3196 does not have a crystal complex structure, we first carried out molecular docking to generate its binding pose in the active pocket of LBD. The three-dimensional structure of MGL-3196 was retrieved from the PubChem database<sup>29</sup> (<https://pubchem.ncbi.nlm.nih.gov/>). Then, the molecular structure was prepared using the openbabel tool.<sup>30</sup> The ion state of MGL-3196 was generated at pH 7.0. As indicated by the study of MGL-3196 optimization,<sup>14</sup> the amide nitrogen atom of the azauracil ring in MGL-3196 is negatively monovalent, thus simulating the carboxylic acid structure of thyroid hormone T3. Then, we used the Autodock Vina method<sup>31</sup> to dock MGL-3196 to the ligand-binding pocket of 1N46. For comparison, T3 was also docked to 1N46. During this process, the ligand in the crystal structure was used as a reference, and amino acids within a range of 10 Å around the pocket were used as pocket residues to generate 10 docking conformations. As a result, the best-scoring docking conformation was consistent with the binding mode of the crystal ligand.

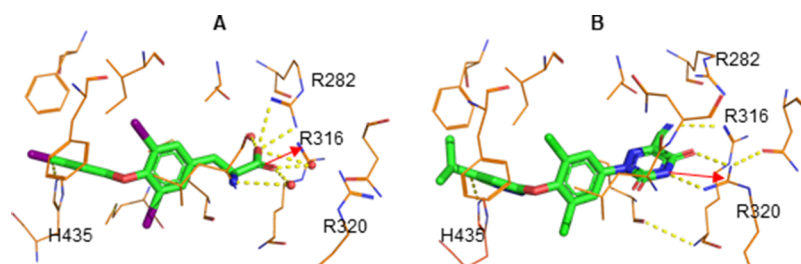


**Figure 2.** (A,B) Binding mode of T3 and MGL-3196. The amino acids within the range of 4 Å around the ligand are represented by brown lines, and the ligand is shown as green sticks. Hydrogen bonds are represented by yellow dashed lines. The red sword represents a salt bridge. The key amino acids involved in the hydrogen bond interaction are labeled with residue names.

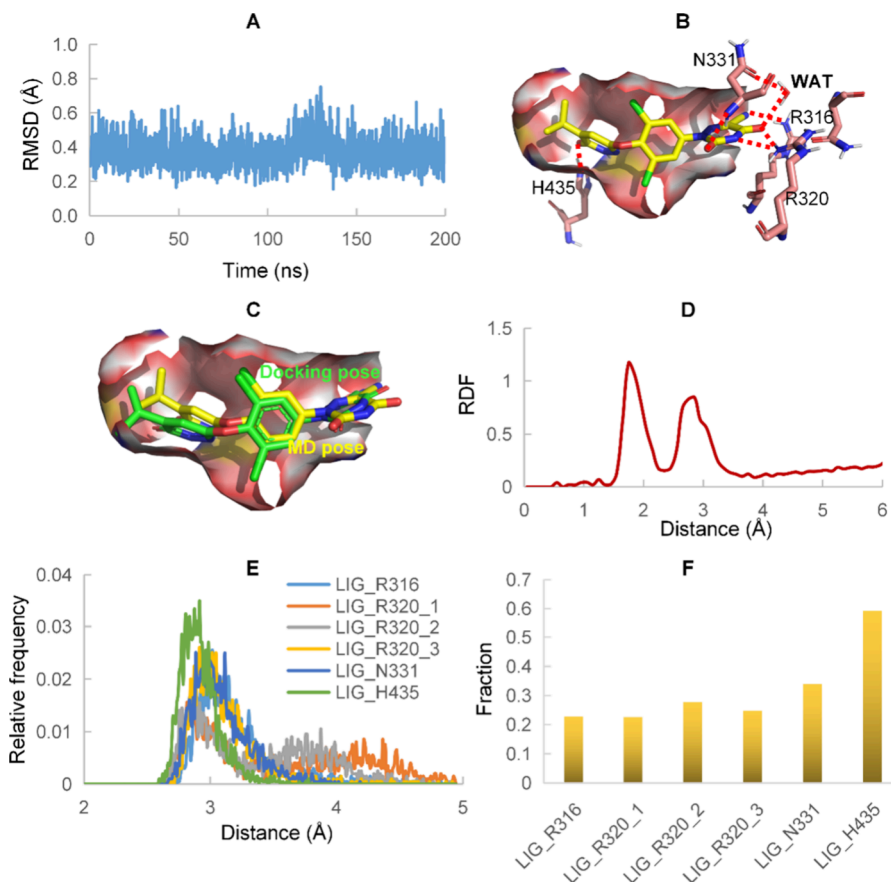


**Figure 3.** (A) RMSD of heavy atoms in MGL-3196 along the simulation time, with the *x*-axis representing the simulation time and the *y*-axis representing the RMSD value (Å). (C) overlapping between the binding pose of MGL-3196 by molecular docking and the binding pose obtained after simulation of 200 ns, and the ligand-binding pocket is represented by a van der Waals surface. (B) Binding mode of MGL-3196 averaged on the conformations in the last 10 ns of simulation. The amino acids within a range of 4 Å around the ligand are represented by light-pink sticks, while the ligand appears as yellow sticks. Hydrogen bonds are represented by red dashed lines. The key amino acids involved in the interaction are labeled with their residue names. (D) Radial distribution of waters around the O6 atom in MGL-3196. The *x*-axis represents the distance between the water atom and the O6 atom. The *y*-axis represents the probability density of the distribution donated as RDF. (E) Distance distribution of hydrogen bonds. (F) fraction of simulation frames that maintain the hydrogen bonds with R316, R320, N331, and H435.

Therefore, we used this conformation for molecular dynamic simulation.

**2.3. Molecular Dynamic Simulation.** We applied GROMACS simulation software<sup>32</sup> to simulate the binding of T3 and MGL-3196 to TR $\beta$ . First, we adopted the semi-empirical method PM3 to generate the point charge information on ligands and set the total molecular charge to  $-1$ . Then, we employed the CHARMM-GUI online service (<https://www.charmm-gui.org>)<sup>33</sup> to prepare simulation systems for simulation. This generated the molecular topology files required for the GROMACS simulation. The protein force

field for simulation is AMBER FF19SB,<sup>34</sup> and the small-molecule ligand force field adopts GAFF2.<sup>35</sup> The simulation was divided into three steps: the first step is the energy optimization stage, with an optimization step of 5000, which limits the protein and ligand coordinates during the optimization process; the second step is a constant temperature and volume (NVT) simulation, which is used to adjust the density of the system. The simulation duration is 300 ps, and the simulation step is 1 fs; and the third step is constant temperature and pressure (NPT) simulation, which is used to generate the required molecular trajectories for research. The

simulation duration is 200 ns and the simulation step is 2 fs. The SHAKE method<sup>36</sup> was used to limit the vibration of hydrogen atoms. Finally, molecular dynamics trajectories were analyzed to obtain information such as root-mean-square deviation (RMSD) and root-mean-square fluctuation (RMSF) of protein backbone atoms, radial distribution function, radius of gyration, intermolecular hydrogen bond, and protein helix content. The binding free energy was computed using the MM-GBSA method.<sup>37</sup>

### 3. RESULTS AND DISCUSSION

**3.1. Binding Model Analysis of MGL-3196 Based on Molecular Docking.** The LBD of TR $\beta$  is composed of 12 helices (Figure S2A). Among them, helices H3, H5, H6, H7, H11, and H12, as well as the loop region between H2 and H3, form the ligand-binding pocket for thyroid hormones. MGL-3196 was docked into this pocket with a docking score of  $-9.7$  kcal/mol. Compared to the crystal binding pose of T3, these two compounds present a similar binding orientation (Figure S2B) despite the substantial structural differences. Both are embedded in the ligand-binding pocket via aromatic rings. However, the hydrogen bonds formed by these two compounds are distinct (Figure 2A,B). Apart from the common hydrogen bond with residue H435, the hydrogen bond formed by the carboxyl group of T3 and the guanidine side chain of R282 is not present in the docking conformation of MGL-3196. At this position, the docking model indicates that MGL-3196 forms a hydrogen bond with R316 through the nitrile group while also forming two hydrogen bonds with the guanidine group of R320 via a lactam structure in the azacytosine ring. Specifically, the lactam O and N atoms each form a hydrogen bond with two different N atoms of the guanidine group, which we refer to as a bidentate hydrogen bond. In this context, the lactam N atom in MGL-3196 is presumed to carry a negative charge at a pH of 7.0. This charged atom then undergoes a salt bridge interaction with the positively charged guanidine group of R320 (Figure S2C). This type of interaction also exists between the carboxyl group of T3 and the guanidine groups of R316 and R320 (Figure S2D). Notably, the carboxyl group of T3 forms an additional hydrogen bond with the crystal water adjacent to T3, which was not observed in the binding of the MGL-3196 derivative in 1N46. The hydrogen bonds between T3 and the crystal water are supplanted by the salt bridge between MGL-3196 and R320. In summary, MGL-3196 replicates the majority of interactions in the binding of T3 to some extent, thereby explaining its capacity to activate TR $\beta$ .

**3.2. Binding Dynamics of MGL-3196.** Starting from the docking conformation of MGL-3196, we conducted 200 ns of molecular dynamic simulation using the complex structure of wild-type TR $\beta$ . Trajectory analysis shows that the RMSD of MGL-3196 exhibits minor fluctuations during the simulation (Figure 3A), indicating that the ligand is highly stable in the pocket. The average RMSD value remains below 0.5 Å, indicating that the ligand conformation obtained by simulation is basically consistent with the initial docking conformation. Extending the simulation time to 400 ns shows the same trend (Figure S3A). This to some extent confirms the correctness of the molecular docking conformation as incorrect conformation often leads to unstable binding.

Subsequently, the average conformation within the last 10 ns of the simulation was extracted (Figure 3B), which demonstrated a high overlap with the docking pose, further

validating the binding stability of MGL-3196 (Figure 3C). In this conformation, it was observed that the hydrogen bond mediated by H435 persists. The hydrogen bond with R316 formed by the nitrile group in the docking pose was also retained in the simulation. Nevertheless, the hydrogen bonds with R320 transformed to a monodentate form, wherein both hydrogen bonds originate from the same N atom of the guanidine group. Additionally, in comparison to the docking model, the lactam group of MGL-3196 formed a novel hydrogen bond with the backbone NH of N331 (Figure S3B). It is worthy of mention that a water molecule was found to form hydrogen bonds with both MGL-3196 and N331. However, such a water molecule was not observed in the crystal structure of 1N46, which harbors a ligand with the same ring structure as MGL-3196. To confirm this observation, the radial distribution of coordinated waters to the O6 atom of MGL-3196, which forms hydrogen bonds with the water molecule, was analyzed, revealing two peaks at distances shorter than 3.0 Å (Figure 3D), indicating the presence of at least one water molecule in this locale. Simultaneously, the side chain of N311 shifted toward the waters, while the side chains of R320 and N233 deviated from the ligand, creating space for the waters, which closely resembled the crystal structure of T3 binding (Figure S3C). The radial distribution analysis demonstrated that water was also enriched in the vicinity of the carboxyl group of T3 in the simulations of both the water-free and water-incorporated molecular systems (Figure S3E,F). Furthermore, a similar distribution was observed around both O atoms within the carboxyl group, suggesting the potential presence of a water network in this region, with multiple waters potentially located at a distance suitable for interaction with T3.

To investigate the stability of the above-mentioned hydrogen bonds, we analyzed their distance distribution in the simulation (Table S1). As shown in Figure 3E, LIG\_H435 has the highest peak at the distance range facilitating ligand binding, indicating that the hydrogen bond with H435 is the most stable one. R320 can make different forms of hydrogen bonds with the ligand. The monodentate form denoted by LIG\_320\_1 has a comparable distribution with the didentate form denoted by R320\_2. These two forms seem to appear alternatively at the state of ligand binding according to the distance fluctuation along the simulation time (Figure S3D). LIG\_320\_3 participates in both monodentate and didentate hydrogen bonds, thus with a higher peak than LIG\_320\_1 and LIG\_320\_2. LIG\_R316 and LIG\_331 representing the hydrogen bonds with R316 and N331 seem to be as stable as those with R320 according to the distance distribution curves. To more accurately assess the importance of hydrogen bonds, we calculated the proportion of frames in the simulation that meet the hydrogen bonding requirements (Figure 3F), where the distance between atoms that mediates the hydrogen bond should be smaller than 3.0 Å. The result is almost consistent with the distance distribution analysis. H435-mediated hydrogen bond exists in over 60% of simulation time. The second one (around 30%) is LIG\_N331, referring to the hydrogen bond with N331, while the rest of the hydrogen bonds exist in at least 20% frames. As shown in the docking model, a salt bridge is also formed between MGL-3196 and R320. The salt bridge interaction is suggested to be very stable for MGL-3196 because the atoms in R320 that mediate the salt bridge are also responsible for the hydrogen bonds with MGL-3196. However, the salt bridges between T3 and R316 and

R320 in the crystal structure are both disrupted by the simulation (Figure S4A,B).

In addition, we calculated the average binding free energy of MGL-3196 using the frames extracted from the trajectory of the last 50 ns (Table 1). The binding free energy based on the

**Table 1. Binding Free Energy Calculation ( $\Delta G$ ) by MM-GBSA**

compound	VDW <sup>a</sup>	EEL <sup>b</sup>	$\Delta G_{\text{sol}}^c$	$\Delta S^d$	$\Delta G$
MGL-3196	-61.30	29.34	-30.98	-21.12	-41.82
T3	-58.40	12.61	-8.64	-26.25	-28.18

<sup>a</sup>VDW represents the van der Waals term. <sup>b</sup>EEL represents the electrostatic term. <sup>c</sup> $\Delta G_{\text{sol}}$  represents the solvation free energy <sup>d</sup> $\Delta S$  represents the entropic term.

simulation of the docking model of T3 with 1N46 was calculated for comparison. The result shows that MGL-3196 has a higher binding affinity than T3. However, a cell-free coactivator recruitment assay suggests that the activation of TR $\beta$  by MGL-3196 ( $EC_{50} = 0.21 \mu\text{M}$ ) is weaker than T3 ( $EC_{50} = 0.015 \mu\text{M}$ ),<sup>14</sup> indicating that the binding affinity of the ligand is not a determining factor for activity because similar situations also exist for other TR ligands.<sup>38</sup> So, it is more important to reveal the activation mechanism of MGL-3196 on TR $\beta$ .

**3.3. Impact of MGL-3196 on Protein Activation.** We investigated whether the stable binding of MGL-3196 would impact the conformation of TR $\beta$ . RMSD analysis of the backbone atoms of the protein reveals that the protein structure with MGL-3196 is more stable than the apo structure (Figure 4A), suggesting that the binding of MGL-3196 can stabilize the protein. Compared with T3, the binding of MGL-3196 leads to a more stable overall protein (Figure 4B). This is also supported by the RMSD values of the ligands (Figure 4C), indicating that MGL-3196 is bound more stably than T3.

Furthermore, the binding of MGL-3196 results in a more compact protein based on the radius of gyration of the protein (Figure 4D), generally contributing to an overall increase in protein stability.

To this end, we will focus on the structural flexibility of the protein to reveal the activation mechanism of MGL-3196. RMSF serves as a crucial metric for assessing residue flexibility, where a higher RMSF value corresponds to increased flexibility. As evident from the RMSF analysis depicted in Figure 5A, the flexibility of helices H3, H4, and H12, which are integral to the formation of the AF-2 site, is enhanced in the MGL-3196 binding state compared to that in the T3-binding state. This region serves as a critical domain for the recruitment of coactivators, and its stability is of utmost importance for the binding of coactivators. This potentially explains why the activity of MGL-3196 is inferior to that of T3. Indeed, studies have demonstrated that there is no inherent correlation between the potency of nuclear receptor agonists and the binding affinity of ligands.<sup>39</sup> Consequently, the stability of the AF-2 conformation has emerged as a key metric for assessing the efficacy of the agonists.

Given that the conformation of H12 (aa 453–459) plays a decisive role in the formation of coactivator-binding sites,<sup>40,41</sup> we conducted further structural analysis on it. The small RMSD value of H12 (Figure 5B) reveals that the conformation of H12 under the binding of MGL-3196 and T3 is basically consistent with the active conformation in the crystal structure. Although the RMSD value of T3 shows a slight increase in simulation, the curve converges in the last 50 ns. More importantly, the small fluctuation of RMSD indicates high stability of H12. It is worth noting that the RMSD value of H12 under the binding of T3 is slightly larger than that for MGL-3196. This is actually not contradictory with the result of RMSF analysis, which reveals that H12 has lower flexibility under the binding of T3 because the fluctuation amplitude in RMSD is much smaller than the positional fluctuation in

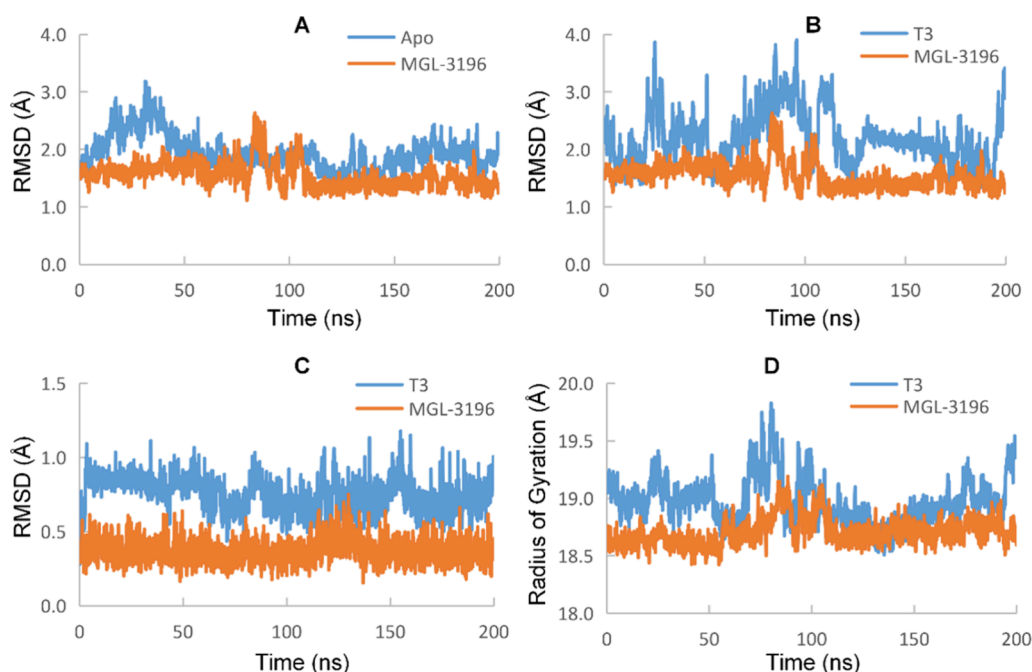


**Figure 4.** (A) RMSD of the protein backbone atoms in the apo and MGL-3196-bound structures. (B) RMSD of the protein backbone atoms in the T3 and MGL-3196-bound structures. (C) RMSD of T3 and MGL-3196. (D) Radius of gyration for T3 and MGL-3196-bound protein.

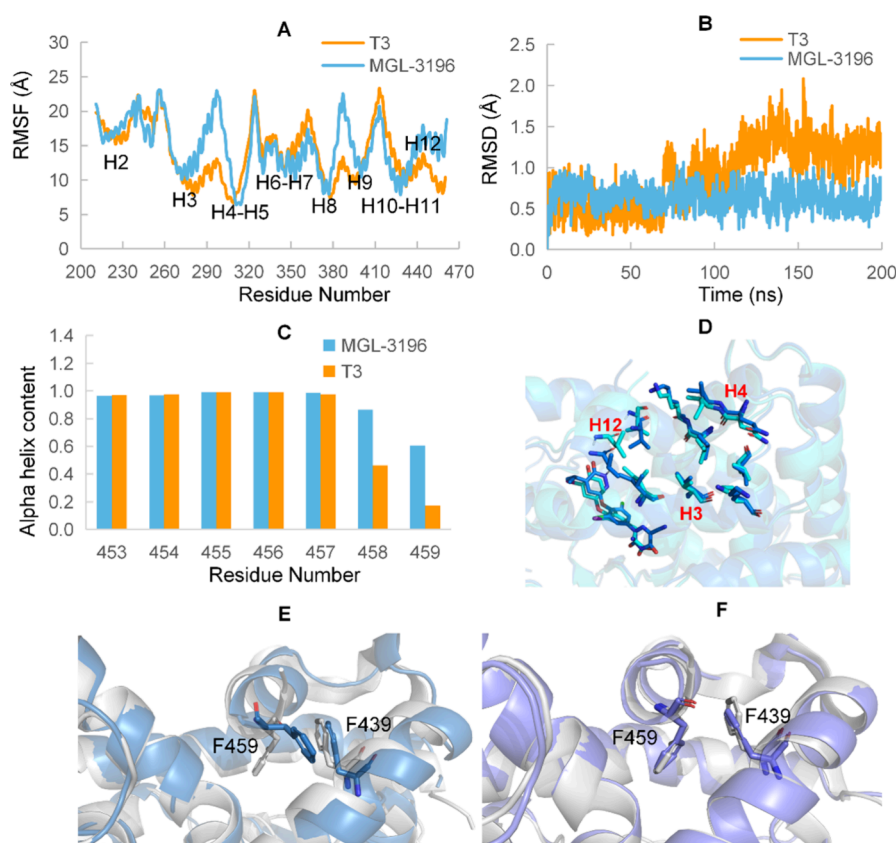


**Figure 5.** (A) Backbone RMSF of each residue in the protein, with residue number on the horizontal axis and RMSF value on the vertical axis. (B) RMSD of protein backbone atoms in helix H12 along the simulation time. (C) Proportion of residues in H12 that exist in a helical form across the whole simulation period. (D) AF-2 residues are displayed as sticks, with blue indicating MGL-3196 binding protein and cyan indicating T3-binding protein. (E,F) Conformational overlapping of F459 and F439 in the simulated structure with the conformation in the crystal structure. The residues are displayed in sticks. The secondary structure of the protein is shown as cartoons. The T3-binding state is colored in blue (E), the MGL-3196 binding state is colored in purple (F), and the crystal structure is colored in gray.

RMSF. The RMSD value mainly reflects the difference between the simulation and the initial conformation and is not necessarily related to the flexibility of residues. On the other hand, the helix content of most residues in H12 approximates 100% for both MGL-3196 and T3 (Figure 5C), which has been reported to be important for TR $\beta$  activation. By comparing the representative conformation obtained by structural clustering on the last 50 ns trajectory, the residues involved in the formation of AF-2 site expose the hydrophobic surface of AF-2 site to the solvent in both MGL-3196 and T3-bound structures (Figure 5D), which is conducive to the binding of coactivators. The difference lies in two residues at the tail of H12, in particular F459. The aromatic side chain of F459 in the T3-bound structure forms a strong PI–PI interaction with the aromatic side chain of F439 on H11 (Figure 5E), but this interaction is not observed in MGL-3196-bound structure (Figure 5F). The formation of this interaction may enhance the stability of helix H12, which explains the higher activity of T3.

**3.4. Effects of Mutations on Protein Activation under the Binding of MGL-3196.** There are multiple mutants in TR $\beta$ , and we chose three mutants from different regions of the LBD (Figure 6A). The H435R mutation is located in the ligand-binding pocket of LBD, and the hydrogen bond formed between this residue and MGL-3196 is crucial for the binding of MGL-3196. Mutating this residue will undoubtedly have a significant impact on ligand binding. R243Q and R338W are

located in the L2/L3 loop and helix H6, respectively. These two residues are located at the periphery of the ligand-binding pocket and do not directly participate in ligand binding. In clinical practice, these residue mutations exhibit hormone resistance, and studying the impact of these mutations on the activation capability of MGL-3196 is of great significance.

RMSD analysis shows that compared to the binding state of MGL-3196 in the wild-type protein, these mutations cause changes in protein conformation and enable the fluctuation of RMSD values greater than that of the wild-type protein (Figure 6B), indicating an increase in the whole protein flexibility. Both RMSD and RMSF analyses reveal that the H12 flexibility of the R338W mutant is comparable to that of the wild-type protein (Figure 6C), suggesting minor effects of this mutation on the activation of TR $\beta$  by MGL-3196. In the R243Q mutant, H12 has lower RMSF than that in the wild-type protein. However, RMSD analysis of the H12 helix shows that R243Q causes the structure of H12 to deviate from that of the wild-type conformation (Figure 6D). H435R makes a similar conformational deviation of H12, and it even increases the RMSF of H12. These results imply that both R243Q and H435R mutation may have a significant impact on the activation capability of MGL-3196. Moreover, these two mutations result in a significant decrease in the helix content of H12, suggesting that these two mutations may be detrimental to the effect of MGL-3196 on TR $\beta$  activation. Furthermore, we compared the conformation of residues

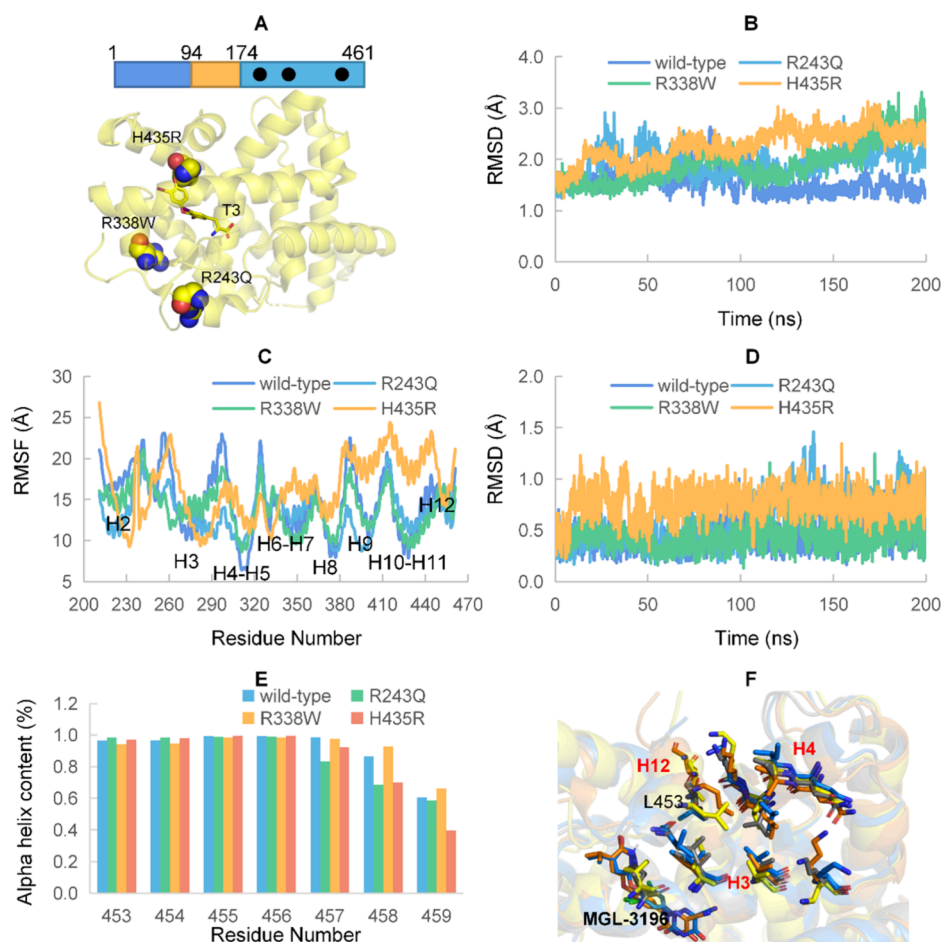


**Figure 6.** (A) Mutation sites in TR $\beta$ . The protein is shown as cartoons. (B) Backbone RMSD of wild-type and mutant systems. (C) Backbone RMSF of residues are in the wild-type and mutant systems. (D) Backbone RMSD of H12 in the wild-type and mutant systems. (E) Proportion of residues in H12 that exist in a helical form in the simulation process. (F) AF-2 residues in the wild-type and mutant systems. Blue sticks represent the AF-2 residues in wild-type protein, and orange, green, and yellow sticks represent those in the R243Q, R338W, and H435R mutants, respectively.

forming the AF-2 site in the representative structure of simulation and found that mutations in R243Q and H435R induce the hydrophobic side chains of L453 in H12 to extend toward the binding cavity of TR $\beta$  coactivator at the AF-2 site. This may hinder the binding of the coactivator and result in MGL-3196 being unable to activate TR $\beta$ . In other words, the R243Q and H435R mutants may enable TR $\beta$  insensitive to MGL-3196, although further experimental verification is needed. The reduced flexibility of H3, H4, and H12 helices in the R243Q mutant could further enhance such resistance. On the contrary, L453 maintains a wild-type-like conformation in the R338W mutant, whose hydrophobic surface of the AF-2 site is still exposed to solvent, indicating that MGL-3196 keeps sensitivity to this mutant. Overall, it can be concluded that TR $\beta$  mutations in the ligand-binding pocket and noncore regions of LBD can both affect the activity of MGL-3196. Therefore, it is necessary to conduct systematic research on how different mutations affect the activity of MGL-3196 in clinical practice in the future, in order to screen out patients who are sensitive to MGL-3196 and to achieve true precision treatment.

#### 4. CONCLUSIONS

This study performed molecular dynamic simulations to investigate the activation mechanism of TR $\beta$  agonist MGL-

3196 which has achieved significant breakthroughs in clinical research. Meanwhile, we also investigated the effects of three typical mutants on the activation activity of MGL-3196. The results indicate that MGL-3196 has an activation mechanism similar to endogenous thyroid hormone T3, which is activated by stabilizing the helical conformation of H12 and promoting the formation of AF-2 coactivator-binding site to activate TR $\beta$ . Simulation of mutant proteins complexed with MGL-3196 shows that the mutants have various sensitivities to MGL-3196. In this study, the H435R mutation in the LBD and the R243Q mutation in the L2/L3 loop region may be resistant to MGL-3196 because both lead to a decrease in H12 helicity and blocked AF-2 coactivator-binding site by the side chain of L453. Conversely, R338W on helix H6 has a relatively minor influence on the activation capability of MGL-3196. Therefore, it is crucial to identify TR $\beta$  mutations that are sensitive to MGL-3196 in clinical medication. In summary, this study successfully clarified the activation mechanism of MGL-3196 and identified mutations in TR $\beta$  that may be resistant to MGL-3196. This enhances the accuracy of patient medication in TR $\beta$ -targeted clinical treatments. Furthermore, the development of new TR $\beta$  agonists that can respond to pan-mutations is necessary to expand the beneficiary population.

## ■ ASSOCIATED CONTENT

### SI Supporting Information

The Supporting Information is available free of charge at <https://pubs.acs.org/doi/10.1021/acsomega.4c00089>.

Table with the definition of hydrogen bonds with MGL-3196; figures regarding ligand structure, protein secondary structure, and various interaction information including water-mediated interactions in the binding pocket (PDF)

## ■ AUTHOR INFORMATION

### Corresponding Authors

**Yi Lu** – Fujian Key Laboratory of Neonatal Diseases, Xiamen Key Laboratory of Neonatal Diseases, Xiamen Children's Hospital (Children's Hospital of Fudan University at Xiamen), Xiamen 361006, China; Department of Pediatrics, Children's Hospital of Fudan University, Shanghai 201102, China; [orcid.org/0000-0002-6504-9548](https://orcid.org/0000-0002-6504-9548); Email: [papamaker@126.com](mailto:papamaker@126.com)

**Liling Qian** – Fujian Key Laboratory of Neonatal Diseases, Xiamen Key Laboratory of Neonatal Diseases, Xiamen Children's Hospital (Children's Hospital of Fudan University at Xiamen), Xiamen 361006, China; Division of Pulmonary Medicine, Shanghai Children's Hospital, School of Medicine, Shanghai Jiao Tong University, Shanghai 200062, China; Email: [lqian@126.com](mailto:lqian@126.com)

### Authors

**Chun Chen** – Fujian Key Laboratory of Neonatal Diseases, Xiamen Key Laboratory of Neonatal Diseases, Xiamen Children's Hospital (Children's Hospital of Fudan University at Xiamen), Xiamen 361006, China

**Deyi Zhuang** – Fujian Key Laboratory of Neonatal Diseases, Xiamen Key Laboratory of Neonatal Diseases, Xiamen Children's Hospital (Children's Hospital of Fudan University at Xiamen), Xiamen 361006, China

Complete contact information is available at:

<https://pubs.acs.org/doi/10.1021/acsomega.4c00089>

### Author Contributions

Y.L. carried out the study and wrote the manuscript under the supervision of L.L.Q. C.C. provided help on the manuscript writing. D.Y.Z. participated in project administration. All authors have read and agreed to the published version of the manuscript.

### Funding

This work was supported by grants from the Fujian Provincial Health Talent Project (2019-ZQNB-35), the Science and Technology Program of Xiamen (3502Z20194086), and the National Natural Science Foundation of China (81903691).

### Notes

The authors declare no competing financial interest.

## ■ ACKNOWLEDGMENTS

We appreciate the help of Dr. Ran in Guangzhou Laboratory (Guangdong, China) for simulation guidance.

## ■ REFERENCES

(1) Flamant, F.; Baxter, J. D.; Forrest, D.; Refetoff, S.; Samuels, H.; Scanlan, T. S.; Vennström, B.; Samarut, J. International Union of Pharmacology. LIX. The pharmacology and classification of the

nuclear receptor superfamily: thyroid hormone receptors. *Pharmacol. Rev.* **2006**, *58* (4), 705–711.

(2) Kowalik, M. A.; Perra, A.; Pibiri, M.; Cocco, M. T.; Samarut, J.; Plateroti, M.; Ledda-columbano, G. M.; Columbano, A. TR beta is the critical thyroid hormone receptor isoform in T3-induced proliferation of hepatocytes and pancreatic acinar cells. *Journal of hepatology* **2010**, *53* (4), 686–692.

(3) Volkov, L. I.; Kim-han, J. S.; Saunders, L. M.; Poria, D.; Hughes, A. E. O.; Kefalov, V. J.; Parichy, D. M.; Corbo, J. C. Thyroid hormone receptors mediate two distinct mechanisms of long-wavelength vision. *Proc. Natl. Acad. Sci. U.S.A.* **2020**, *117* (26), 15262–15269.

(4) Yen, P. M. Physiological and molecular basis of thyroid hormone action. *Physiol. Rev.* **2001**, *81* (3), 1097–1142.

(5) Hennemann, G.; Docter, R.; Friesema, E. C.; De jong, M.; Krenning, E. P.; Visser, T. J. Plasma membrane transport of thyroid hormones and its role in thyroid hormone metabolism and bioavailability. *Endocrine reviews* **2001**, *22* (4), 451–476.

(6) Cheng, S. Y.; Leonard, J. L.; Davis, P. J. Molecular aspects of thyroid hormone actions. *Endocrine reviews* **2010**, *31* (2), 139–170.

(7) Mandato, C.; D'acunzo, I.; Vajro, P. Thyroid dysfunction and its role as a risk factor for non-alcoholic fatty liver disease: What's new. *Digestive and liver disease: official journal of the Italian Society of Gastroenterology and the Italian Association for the Study of the Liver* **2018**, *50* (11), 1163–1165.

(8) Chung, G. E.; Kim, D.; Kim, W.; Yim, J. Y.; Park, M. J.; Kim, Y. J.; Yoon, J. H.; Lee, H. S. Non-alcoholic fatty liver disease across the spectrum of hypothyroidism. *Journal of hepatology* **2012**, *57* (1), 150–156.

(9) Alonso-merino, E.; Martín orozco, R.; Ruíz-llorente, L.; Martínez-iglesias, O. A.; Velasco-martín, J. P.; Montero-pedrazuela, A.; Fanjul-rodríguez, L.; Contreras-jurado, C.; Regadera, J.; Aranda, A. Thyroid hormones inhibit TGF- $\beta$  signaling and attenuate fibrotic responses. *Proc. Natl. Acad. Sci. U.S.A.* **2016**, *113* (24), E3451–60.

(10) Baerenthaler, T.; Ding, S.; Chioccioli, M.; Poli, F.; Justet, A.; Rose, K.-A.; Cosme, C. Jr.; Adams, T.; Ahangari, F.; Rosas, I. O.; Kaminski, N. Antifibrotic Effects of Sobetirome, a Thyroid Hormone Receptor Beta Agonist. *Am. J. Respir. Crit. Care Med.* **2022**, *205*, A3722–A3722, DOI: [10.1164/ajrccm-conference.2022.205.1\\_MeeetingAbstracts.A3722](https://doi.org/10.1164/ajrccm-conference.2022.205.1_MeeetingAbstracts.A3722).

(11) Borngraeber, S.; Budny, M. J.; Chiellini, G.; Cunha-lima, S. T.; Togashi, M.; Webb, P.; Baxter, J. D.; Scanlan, T. S.; Fletterick, R. J. Ligand selectivity by seeking hydrophobicity in thyroid hormone receptor. *Proc. Natl. Acad. Sci. U.S.A.* **2003**, *100* (26), 15358–15363.

(12) Erion, M. D.; Cable, E. E.; Ito, B. R.; Jiang, H.; Fujitaki, J. M.; Finn, P. D.; Zhang, B. H.; Hou, J.; Boyer, S. H.; Van poelje, P. D.; Linemeyer, D. L. Targeting thyroid hormone receptor-beta agonists to the liver reduces cholesterol and triglycerides and improves the therapeutic index. *Proc. Natl. Acad. Sci. U.S.A.* **2007**, *104* (39), 15490–15495.

(13) Boyer, S. H.; Jiang, H.; Jacintho, J. D.; Reddy, M. V.; Li, H.; Li, W.; Godwin, J. L.; Schulz, W. G.; Cable, E. E.; Hou, J.; Wu, R.; Fujitaki, J. M.; Hecker, S. J.; Erion, M. D. Synthesis and biological evaluation of a series of liver-selective phosphonic acid thyroid hormone receptor agonists and their prodrugs. *Journal of medicinal chemistry* **2008**, *51* (22), 7075–7093.

(14) Kelly, M. J.; Pietranico-cole, S.; Larigan, J. D.; Haynes, N.-E.; Reynolds, C. H.; Scott, N.; Vermeulen, J.; Dvorozniak, M.; Condeknape, K.; Huang, K.-S.; So, S.-S.; Thakkar, K.; Qian, Y.; Banner, B.; Mennona, F.; Danzi, S.; Klein, I.; Taub, R.; Tilley, J. Discovery of 2-[3,5-Dichloro-4-(5-isopropyl-6-oxo-1,6-dihydropyridazin-3-yloxy)-phenyl]-3,5-dioxo-2,3,4,5-tetrahydro[1,2,4]triazine-6-carbonitrile (MGL-3196), a Highly Selective Thyroid Hormone Receptor  $\beta$  Agonist in Clinical Trials for the Treatment of Dyslipidemia. *Journal of medicinal chemistry* **2014**, *57* (10), 3912–3923.

(15) Berkenstam, A.; Kristensen, J.; Mellström, K.; Carlsson, B.; Malm, J.; Rehnmark, S.; Garg, N.; Andersson, C. M.; Rudling, M.; Sjöberg, F.; Angelin, B.; Baxter, J. D. The thyroid hormone mimetic compound KB2115 lowers plasma LDL cholesterol and stimulates

- bile acid synthesis without cardiac effects in humans. *Proc. Natl. Acad. Sci. U.S.A.* **2008**, *105* (2), 663–667.
- (16) Ladenson, P. W.; Kristensen, J. D.; Ridgway, E. C.; Olsson, A. G.; Carlsson, B.; Klein, I.; Baxter, J. D.; Angelin, B. Use of the thyroid hormone analogue eprotirome in statin-treated dyslipidemia. *New England journal of medicine* **2010**, *362* (10), 906–916.
- (17) Harrison, S. A.; Bashir, M. R.; Guy, C. D.; Zhou, R.; Moylan, C. A.; Frias, J. P.; Alkhoury, N.; Bansal, M. B.; Baum, S.; Neuschwander-tetri, B. A.; Taub, R.; Moussa, S. E. Resmetirom (MGL-3196) for the treatment of non-alcoholic steatohepatitis: a multicentre, randomised, double-blind, placebo-controlled, phase 2 trial. *Lancet (London, England)* **2019**, *394* (10213), 2012–2024.
- (18) Concolino, P.; Costella, A.; Paragliola, R. M. Mutational Landscape of Resistance to Thyroid Hormone Beta (RTH $\beta$ ). *Molecular diagnosis & therapy* **2019**, *23* (3), 353–368.
- (19) Hassan, A. Q.; Koh, J. T. A functionally orthogonal ligand-receptor pair created by targeting the allosteric mechanism of the thyroid hormone receptor. *J. Am. Chem. Soc.* **2006**, *128* (27), 8868–8874.
- (20) Hassan, A. Q.; Koh, J. T. Selective chemical rescue of a thyroid-hormone-receptor mutant, TRbeta(H435Y), identified in pituitary carcinoma and resistance to thyroid hormone. *Angewandte Chemie (International ed. in English)* **2008**, *47* (38), 7280–7283.
- (21) Li, Q.; Yao, B.; Zhao, S.; Lu, Z.; Zhang, Y.; Xiang, Q.; Wu, X.; Yu, H.; Zhang, C.; Li, J.; Zhuang, X.; Wu, D.; Li, Y.; Xu, Y. Discovery of a Highly Selective and H435R-Sensitive Thyroid Hormone Receptor  $\beta$  Agonist. *Journal of medicinal chemistry* **2022**, *65* (10), 7193–7211.
- (22) Fischer, A.; Frehner, G.; Lill, M. A.; Smieško, M. Conformational Changes of Thyroid Receptors in Response to Antagonists. *J. Chem. Inf. Model.* **2021**, *61* (2), 1010–1019.
- (23) Alonso, M.; Goodwin, C.; Liao, X.; Ortega-carvalho, T.; Machado, D. S.; Wondisford, F. E.; Refetoff, S.; Weiss, R. E. In vivo interaction of steroid receptor coactivator (SRC)-1 and the activation function-2 domain of the thyroid hormone receptor (TR) beta in TRbeta E457A knock-in and SRC-1 knockout mice. *Endocrinology* **2009**, *150* (8), 3927–34.
- (24) Burley, S. K.; Bhikadiya, C.; Bi, C.; Bittrich, S.; Chen, L.; Crichlow, G. V.; Duarte, J. M.; Dutta, S.; Fayazi, M.; Feng, Z.; Flatt, J. W.; Ganesan, S. J.; Goodsell, D. S.; Ghosh, S.; Kramer green, R.; Guranovic, V.; Henry, J.; Hudson, B. P.; Lawson, C. L.; Liang, Y.; Lowe, R.; Peisach, E.; Persikova, I.; Piehl, D. W.; Rose, Y.; Sali, A.; Segura, J.; Sekharan, M.; Shao, C.; Vallat, B.; Voigt, M.; Westbrook, J. D.; Whetstone, S.; Young, J. Y.; Zardecki, C. RCSB Protein Data Bank: Celebrating 50 years of the PDB with new tools for understanding and visualizing biological macromolecules in 3D. *Protein science: a publication of the Protein Society* **2022**, *31* (1), 187–208.
- (25) Nascimento, A. S.; Dias, S. M.; Nunes, F. M.; Aparício, R.; Ambrosio, A. L.; Bleicher, L.; Figueira, A. C.; Santos, M. A.; De oliveira neto, M.; Fischer, H.; Togashi, M.; Craievich, A. F.; Garratt, R. C.; Baxter, J. D.; Webb, P.; Polikarpov, I. Structural rearrangements in the thyroid hormone receptor hinge domain and their putative role in the receptor function. *J. Mol. Biol.* **2006**, *360* (3), 586–598.
- (26) Dow, R. L.; Schneider, S. R.; Paight, E. S.; Hank, R. F.; Chiang, P.; Cornelius, P.; Lee, E.; Newsome, W. P.; Swick, A. G.; Spitzer, J.; Hargrove, D. M.; Patterson, T. A.; Pandit, J.; Chrunyk, B. A.; Lemotte, P. K.; Danley, D. E.; Rosner, M. H.; Ammirati, M. J.; Simons, S. P.; Schulte, G. K.; Tate, B. F.; Dasilva-jardine, P. Discovery of a novel series of 6-azauracil-based thyroid hormone receptor ligands: potent, TR beta subtype-selective thymimetics. *Bioorganic & medicinal chemistry letters* **2003**, *13* (3), 379–382.
- (27) Anandkrishnan, R.; Aguilar, B.; Onufriev, A. V. H++ 3.0: automating pK prediction and the preparation of biomolecular structures for atomistic molecular modeling and simulations. *Nucleic Acids Res.* **2012**, *40*, W537–W541.
- (28) Weiss, R. E.; Sadow, P. M., Thyroid Hormone Receptor, TSH and TSH Receptor Mutations. In *Encyclopedia of Hormones*, Henry, H. L.; Norman, A. W., Eds. Academic Press: New York, 2003; pp 477–483.
- (29) Kim, S.; Chen, J.; Cheng, T.; Gindulyte, A.; He, J.; He, S.; Li, Q.; Shoemaker, B. A.; Thiessen, P. A.; Yu, B.; Zaslavsky, L.; Zhang, J.; Bolton, E. E. PubChem 2023 update. *Nucleic acids research* **2023**, *51* (D1), D1373–d1380.
- (30) O'boyle, N. M.; Banck, M.; James, C. A.; Morley, C.; Vandermeersch, T.; Hutchison, G. R. Open Babel: An open chemical toolbox. *J. Cheminf.* **2011**, *3*, 33.
- (31) Eberhardt, J.; Santos-martins, D.; Tillack, A. F.; Forli, S. AutoDock Vina 1.2.0: New Docking Methods, Expanded Force Field, and Python Bindings. *J. Chem. Inf. Model.* **2021**, *61* (8), 3891–3898.
- (32) Van der spoel, D.; Lindahl, E.; Hess, B.; Groenhof, G.; Mark, A. E.; Berendsen, H. J. GROMACS: fast, flexible, and free. *Journal of computational chemistry* **2005**, *26* (16), 1701–1718.
- (33) Jo, S.; Cheng, X.; Lee, J.; Kim, S.; Park, S. J.; Patel, D. S.; Beaven, A. H.; Lee, K. I.; Rui, H.; Park, S.; Lee, H. S.; Roux, B.; Mackerell, A. D., Jr.; Klauda, J. B.; Qi, Y.; Im, W. CHARMM-GUI 10 years for biomolecular modeling and simulation. *Journal of computational chemistry* **2017**, *38* (15), 1114–1124.
- (34) Tian, C.; Kasavajhala, K.; Belfon, K. A. A.; Raguette, L.; Huang, H.; Miguez, A. N.; Bickel, J.; Wang, Y.; Pincay, J.; Wu, Q.; Simmerling, C. ff19SB: Amino-Acid-Specific Protein Backbone Parameters Trained against Quantum Mechanics Energy Surfaces in Solution. *J. Chem. Theory Comput.* **2020**, *16* (1), 528–552.
- (35) He, X.; Man, V. H.; Yang, W.; Lee, T. S.; Wang, J. A fast and high-quality charge model for the next generation general AMBER force field. *J. Chem. Phys.* **2020**, *153* (11), 114502.
- (36) Ryckaert, J.-P.; Ciccotti, G.; Berendsen, H. J. C. Numerical integration of the cartesian equations of motion of a system with constraints: molecular dynamics of n-alkanes. *J. Comput. Phys.* **1977**, *23* (3), 327–341.
- (37) Genheden, S.; Ryde, U. The MM/PBSA and MM/GBSA methods to estimate ligand-binding affinities. *Expert opinion on drug discovery* **2015**, *10* (5), 449–61.
- (38) Gershengorn, M. C.; Geras, E.; Marcus-samuels, B. E.; Rebecchi, M. J. Receptor affinity and biological potency of thyroid hormones in thyrotropic cells. *American journal of physiology* **1979**, *237* (2), E142–6.
- (39) Buchwald, P. A Receptor Model With Binding Affinity, Activation Efficacy, and Signal Amplification Parameters for Complex Fractional Response Versus Occupancy Data. *Front. Pharmacol.* **2019**, *10*, 605.
- (40) Souza, P. C.; Barra, G. B.; Velasco, L. F.; Ribeiro, I. C.; Simeoni, L. A.; Togashi, M.; Webb, P.; Neves, F. A.; Skaf, M. S.; Martinez, L.; Polikarpov, I. Helix 12 dynamics and thyroid hormone receptor activity: experimental and molecular dynamics studies of Ile280 mutants. *Journal of molecular biology* **2011**, *412* (5), 882–893.
- (41) Shizu, R.; Nishiguchi, H.; Tashiro, S.; Sato, T.; Sugawara, A.; Kanno, Y.; Hosaka, T.; Sasaki, T.; Yoshinari, K. Helix 12 stabilization contributes to basal transcriptional activity of PXR. *J. Biol. Chem.* **2021**, *297* (3), 100978.